BAYESIAN AND CRAMÉR-RAO BOUNDS FOR SINGLE SENSOR TARGET LOCALIZATION VIA MULTIPATH EXPLOITATION

Pawan Setlur and Natasha Devroye

University of Illinois at Chicago
Electrical and Computer Engineering Department
Chicago, IL, 60607

ABSTRACT

In urban scenarios, target localization may be achieved using a single sensor via multipath exploitation. The multipath generating mechanisms such as building walls creates virtual radar sensors aiding in localization. For a wide class of radar-target geometries, specialized functions termed multipath preservers are derived to ensure that multipath is physically observable in the radar returns, and therefore these functions assist in evaluating the potential of multipath exploitation in urban sensing. The single sensor system performance is studied by deriving the Cramér-Rao and the Bayesian Cramér-Rao bounds (BCRBs). Given a reflecting geometry, these lower bounds and multipath preservers allow the radar operator to anticipate blind spots, place confidence levels on the localization results, and permit sensor positioning to optimally aid in exploiting multipath for target localization. It is shown here that Cramér-Rao bounds (CRBs) on the location parameters improve with additional multipath.

Index Terms— Target localization, Radar, Multipath Exploitation, Bayesian Cramér-Rao, Urban Sensing, Experimental design.

1. INTRODUCTION

When radar signals are reflected from walls in urban scenarios, multipath radar returns result. Multipath radar returns create virtual radar sensors, permitting noncoherent target localization with a *single sensor,* as demonstrated theoretically and experimentally in [1].

A single target enclosed in a rectangular urban canyon type geometry consisting of three walls is assumed. The walls are assumed to be smooth at the radar operating frequencies, resulting in specular reflections. For lower wavelengths, wall roughness possibly induces diffuse multipath returns [2]-[5],[6], and is not the focus of this paper. In the multipath exploitation literature [1],[6]-[10], it is assumed that multipath returns exist; no such conditions are enforced here. Rather, our formulation is general and incorporates the concept of "multipath preservers", which are functions of the reflecting geometry assumed. Using this general framework, the Cramér-Rao bounds (CRBs) and the Bayesian Cramér-Rao lower bounds (BCRBs) for the target downrange and the crossrange are obtained.

Using the theory of optimal experimental design [11, 12], and employing the multipath preservers, the CRBs and BCRBs allow the radar operator to anticipate blind spots, permit sensor or target positioning, improve interpretability of the radar returns, and place confidence levels on single sensor localization employing multipath exploitation. Note that our focus is not on improving the estimation of the multipath or the direct path time delays, and nor on deriving performance bounds on the time delay estimation [13] and references therein. Rather, the focus is on evaluating single sensor localization performance bounds via multipath exploitation given the actual or the estimates of the direct and multipath time delays.

Prior Work: Multipath exploitation in radar has been reported in the recent literature [7]-[10], all of which assume specular multipath. Statistical radar detection was treated in [7], target tracking in [8], airborne radar applications in [9], range-Doppler application in [6], experimental indoor multipath detection in [10], and localization, but not with a single sensor in [14]. The CRBs on the location parameters using multiple sensors were derived in [14]. Single sensor target localization was studied in [1], but neither the CRBS nor the BCRBS were derived. Multipath in synthetic aperture radar (SAR) was studied in [15]-[17], to deal with SAR multipath ghosts, and noncoherent localization was not the focus of the analysis.

2. MODEL

For ease of exposition we start with a single reflecting surface such as the side wall of a building as shown in Fig. 1(a), in two dimensions, with origin "O", target denoted as (T), radar (R), and the virtual radar created due to the multipath w.r.t wall-1 and denoted as (VR_1) as shown in this figure. The radar and target are located at $\mathbf{x_r} = [-x_r, y_r]^T$ and $\mathbf{x_t} = [-x_t, y_t]^T$. There are three paths, shown in Fig. 1(a), which result in time delays as follows,

$$\tau_1 = 2\frac{||\mathbf{x_t} - \mathbf{x_r}||}{c}, \tau_2 = 2\frac{|\mathbf{x_r^1} - \mathbf{x_t}||}{c}, \tau_3 = \frac{\tau_1 + \tau_2}{2} \quad (1)$$

where c denotes the speed of light in freespace, and $\mathbf{x_r^1} := [x_r; y_r]^T$. The time delays, τ_2 and τ_3 with $\tau_1 \leq \tau_3 \leq \tau_2$, are referred to as the II-order and I-order multipath, respectively. The first order (I-order) multipath incorporates one, while the second-order (II-order) multipath incorporates two reflections at wall-1. Rewriting (1) as

$$(x_t - x_r)^2 + (y_t - y_r)^2 = c^2\tau_1^2/4 \quad (2a)$$

$$(x_t + x_r)^2 + (y_t - y_r)^2 = c^2\tau_2^2/4 \quad (2b)$$

$$\frac{x_t^2}{c^2\tau_3^2/4} + \frac{(y_t - y_r)^2}{(c^2\tau_3^2 - 4x_r^2)/4} = 1. \quad (2c)$$

it is seen that (2a) and (2b) are the equations of circles, whereas (2c) is the equation of an ellipse which has its foci at the radar, $\mathbf{x_r}$ and the *virtual radar* at $\mathbf{x_r^1}$, consistent with a bistatic radar configuration. The intersection point of (2a),(2b),(2c) is the target location $\mathbf{x_t}$, the other intersection is behind the radar and is ignored. When the measured time delays $\tau_i, i = 1, 2, 3$ are substituted in (2), the

This work was sponsored by US AFOSR under award FA9550-10-1-0239; no official endorsement must be inferred.

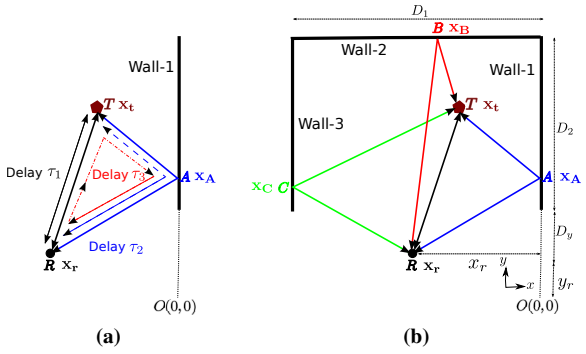

Fig. 1: Radar Scene: (a) Single wall, (b) Urban canyon

target may be noncoherently localized, provided the multipath and direct path time delays are detectable and resolvable in the range profile [1]. The multipath therefore creates *virtual* monostatic and *virtual* bistatic receivers aiding localization with a single *real* monostatic sensor. Now consider Fig. 1(b), which shows an urban canyon type geometry with the dimensions as shown. Denote the multipath time delays generated from wall-2 as τ_4 and τ_5 ($\tau_1 \leq \tau_5 \leq \tau_4$), and wall-3 as τ_6 and τ_7 ($\tau_1 \leq \tau_7 \leq \tau_6$), given by

$$\tau_4 = 2||\mathbf{x_r^2} - \mathbf{x_t}||/c, \tau_5 = \tau_1/2 + \tau_4/2 \quad (3)$$

$$\tau_6 = 2||\mathbf{x_r^3} - \mathbf{x_t}||/c, \tau_7 = \tau_1/2 + \tau_6/2 \quad (4)$$

for *virtual radars* at positions $\mathbf{x_r^2} := [-x_r, 2D_2{+}2D_y{+}y_r]^T, \mathbf{x_r^3} := [-(2D_1 - x_r), y_r]^T$, created by wall-2,3, respectively. The parameter D_y is defined as *standoff distance*.

2.1. Multipath Preservers

Using geometric arguments we derive functions that indicate when multipath is present in the radar returns. In general these functions predict spatial zones where rich multipath may be present, and which could be 'mined' for potential multipath exploitation. For sensor positioning, these functions may be used in a straightforward manner to place spatial constraints on the number of feasible sensor positions, with the objective of maximizing the multipath exploited system performance. Further, these functions could also be used *a posteriori* in placing some confidence on the target location estimates. The formulation in (1) and (3) assumes that multipath returns are always present for each wall and was an implicit assumption in [1]-[14],[15]-[17]. This is in general not true. To understand why, consider point A in Fig. 1(a), having coordinates $\mathbf{x_A} = [0, y_A]^T$, $y_A(\mathbf{x_r}, \mathbf{x_t}) := \frac{y_t x_r + x_t y_r}{x_t + x_r}$ functions of the radar and target coordinates. Clearly, for multipath to exist for this wall, we must have that $D_y + y_r \leqslant y_A \leqslant D_2 + D_y + y_r$. We can now formulate a multipath preserving function, denoted as $f_1(y_A)$,

$$f_1(y_A) = \mathbb{1}[D_y + y_r \leqslant y_A \leqslant D_2 + D_y + y_r], \quad (5)$$

where $\mathbb{1}[\cdot]$ is the indicator function. In essence, (5) implies that if point A is not on its respective wall, then no multipath is observed, which implies $\tau_3 = \tau_2 = 0$. In the same spirit, we may derive the multipath preserving functions for the other two walls in Fig.1(b) as

$$f_2(x_B) = \mathbb{1}[0 \leqslant x_B \leqslant D_1], \quad (6)$$

$$f_3(y_C) = \mathbb{1}[D_y + y_r \leqslant y_C \leqslant D_2 + D_y + y_r], \quad (7)$$

with coordinates $x_B(\mathbf{x_r}, \mathbf{x_t}) := \frac{x_r(D_2+D_y+y_r-y_t)+x_t(D_2+D_y)}{2D_2+2D_y+y_r-y_t}$, $y_C(\mathbf{x_r}, \mathbf{x_t}) := \frac{y_t x_r - y_t D_1 + y_r x_t - y_r D_1}{x_r + x_t - 2D_1}$. The coordinates of points B and C in Fig. 1(b) are then expressed as, $\mathbf{x_B} = [-x_B, D_2 + D_y + y_r]^T$ and $\mathbf{x_C} = [-D_1, y_C]^T$ respectively. The coordinates of the points, A, B, C are functions of both $\mathbf{x_t}$ and $\mathbf{x_r}$.

3. CRAMÉR-RAO AND BAYESIAN CRAMÉR-RAO BOUNDS

In practice, the time delays, $\tau_p,\ p = 1, \ldots 7$ are obtained from correlating the transmitted signal with the received radar returns, see for example [1]. It is therefore reasonable to assume that the measured time delays, denoted as ζ_p are perturbed versions of their true counterparts. The perturbations v_p are assumed to be zero mean, normally distributed and mutually uncorrelated random variables of variance σ_p^2. Thus, the p-th time delay measurement, ζ_p is:

$$\zeta_p = f(p) \times \tau_p + v_p, \quad p = 1, 2, \cdots 7, \quad (8)$$

where $f(1) = 1$, $f(2) = f(3) = f_1(y_A)$, $f(4) = f(5) = f_2(x_B)$, and $f(6) = f(7) = f_3(y_C)$. The assumption of normality imposed on the v_p ensure analytical tractability of the CRBs. If the τ_p are well separated in the τ domain, which is the case for large bandwidth, then the v_p may be modeled as uncorrelated; this is our assumption.

3.1. Cramér-Rao bounds

The Cramér-Rao bound for target localization is given by the inverse of the FIM for target location $\mathbf{x_t}$. We break the complete FIM down into its various components, i.e. first, we examine the FIM considering only the multipath and direct path w.r.t to each wall independently. Let $\mathbf{F}_k(\mathbf{x_t})$ denote the FIM considering only wall $k = 1, 2, 3$ assuming $\mathbf{x_t^1} := [x_t, y_t]^T$, i.e. suppressing the negative sign of x_t in $\mathbf{x_t}$. Using (8) and for the time being assuming that the corresponding multipath preservers are unity,

$$\mathbf{F}_k(\mathbf{x_t}) = \frac{1}{\sigma_1^2}\frac{\partial \tau_1}{\partial \mathbf{x_t^1}}\left(\frac{\partial \tau_1}{\partial \mathbf{x_t^1}}\right)^T + \left(\mathbf{G}_k \odot \frac{\partial \boldsymbol{\tau}_k}{\partial \mathbf{x_t^1}}\right)\left(\mathbf{G}_k \odot \frac{\partial \boldsymbol{\tau}_k}{\partial \mathbf{x_t^1}}\right)^T \quad (9)$$

where,'$\odot$' denotes the Hadamard product, $\boldsymbol{\tau}_k := [\tau_{2k}, \tau_{2k+1}], k = 1, 2, 3$. Furthur $\mathbf{G}_k := \begin{bmatrix} 1/\sigma_{2k} & 1/\sigma_{2k+1} \\ 1/\sigma_{2k} & 1/\sigma_{2k+1} \end{bmatrix}$, $\frac{\partial \boldsymbol{\tau}_k}{\partial \mathbf{x_t^1}} := \left[\left(\frac{\partial \boldsymbol{\tau}_k}{\partial x_t}\right)^T, \left(\frac{\partial \boldsymbol{\tau}_k}{\partial y_t}\right)^T\right]^T \in \Re^{2\times 2}$, $\frac{\partial \tau_1}{\partial \mathbf{x_t^1}} := \left[\frac{\partial \tau_1}{\partial x_t}, \frac{\partial \tau_1}{\partial y_t}\right]^T \in \Re^{2\times 1}$, $\frac{\partial \boldsymbol{\tau}_k}{\partial(\cdot)} := \left[\frac{\partial \tau_{2k}}{\partial(\cdot)}, \frac{\partial \tau_{2k+1}}{\partial(\cdot)}\right] \in \Re^{1\times 2}$. The partial derivatives in (9) are obtained from (1) and (3). The FIM, $\mathbf{F}_k(\mathbf{x_t})$ can now be constructed and is not shown here. It is noted nonetheless, that if any one of the multipath preservers in (5),(6) or (7) is zero, then those corresponding FIMs are rank deficient and hence singular at the corresponding target locations.

The complete FIM incorporating all the multipath time delays and the direct path is given by

$$\mathbf{F}(\mathbf{x_t}) = \frac{1}{\sigma_1^2}\frac{\partial \tau_1}{\partial \mathbf{x_t^1}}\left(\frac{\partial \tau_1}{\partial \mathbf{x_t^1}}\right)^T + \sum_{k=1}^{3}\left(\mathbf{G}_k \odot \frac{\partial \boldsymbol{\tau}_k}{\partial \mathbf{x_t^1}}\right)\left(\mathbf{G}_k \odot \frac{\partial \boldsymbol{\tau}_k}{\partial \mathbf{x_t^1}}\right)^T.$$

From the above equation, it is seen that richer resolvable multipath mechanisms improve the CRBs by adding more statistical information to the FIM. The same conclusion can be made if we were to include higher order multipath from multiple reflections, provided of course they are detectable. We now incorporate the multipath preservers formally into our FIM definitions. Define the regions, $\aleph = \{(-x, y)\,|0 \leq x \leq D_1, D_y + y_r \leq y \leq D_2 + D_y + y_r\}$ and $\aleph_k =$

$\{(-x, y) \in \aleph \,|\, f_k(g_k(x, y)) = 1\}, k = 1, 2, 3$, such that $\aleph_k \subseteq \aleph$, and $g_1(x, y) := y_A(\mathbf{x_r}, (x, y))$, $g_2(x, y) := x_B(\mathbf{x_r}, (x, y))$, and $g_3(x, y) := y_C(\mathbf{x_r}, (x, y))$. In other words, $\aleph$ consists of the entire region inside the urban canyon, and $\aleph_k$ are the regions inside the urban canyon where the corresponding multipath preservers are unity. The FIMs can now be redefined as $\mathbf{F}_k := \mathbf{F}_k(\mathbf{x_t})\mathbb{1}[\mathbf{x_t} \in \aleph_k]$ and $\mathbf{F} := \mathbf{F}(\mathbf{x_t})\mathbb{1}[\mathbf{x_t} \in \bigcup_{k=1}^{3} \aleph_k]$. It is noted that $\mathbf{F}_k$ are evaluated at only those target locations which yield unit values for their corresponding multipath preservers. For all other locations $\mathbf{F}_k$ are rank-1 and hence singular, which implies that unbiased estimation of the target is not possible.

3.2. Bayesian Cramér-Rao Bounds

Assume that prior surveillance has made available the information that the target is located in a certain region inside the urban canyon in Fig. 1(b). In such situations BCRBs [18] are useful in analyzing the system performance.

Assume for simplicity that the the target is uniformly distributed in $(-x_{max}, y_{max}) \times (-x_{min}, y_{min})$ inside the canyon. The joint probability density function of x_t and y_t is then, $p(x_t, y_t) = \frac{\mathbb{1}[(x_t,y_t)\in(x_{max},y_{max})\times(x_{min},y_{min})]}{(x_{max}-x_{min})(y_{max}-y_{min})}$. Let us define the measured time delay vector, $\boldsymbol{\zeta} = [\zeta_1, \ldots, \zeta_7]^T$, and $p(\boldsymbol{\zeta}, x_t, y_t)$ as the joint pdf of $\boldsymbol{\zeta}, x_t$, and y_t. Then the Bayesian information matrix (BIM) which considers multipath from all the walls is

$$\begin{aligned}\mathbf{B} =& \mathbb{E}\left\{\mathbb{E}\left\{-\frac{\partial \ln p(\boldsymbol{\zeta}|(x_t, y_t))}{\partial \mathbf{x_t^1}}\left(\frac{\partial \ln p(\boldsymbol{\zeta}|(x_t, y_t))}{\partial \mathbf{x_t^1}}\right)^T\right\}\right\} \quad (10)\\ &+\mathbb{E}\left\{-\frac{\partial \ln p(x_t, y_t)}{\partial \mathbf{x_t^1}}\left(\frac{\partial \ln p(x_t, y_t)}{\partial \mathbf{x_t^1}}\right)^T\right\}\\ =&\mathbb{E}\left\{\mathbf{F}(x_t, y_t)\right\} + \mathbf{0} = \iint_{x_t=x_{min}, y_t=y_{min}}^{x_{max}, y_{max}} \mathbf{F}(x_t, y_t)\, \mathrm{d}x_t\, \mathrm{d}y_t.\end{aligned}$$

The zero matrix in (10) arises as the joint pdf $p(x_t, y_t)$ is a non-informative prior. For other prior distributions assumed, the second term will be nonzero. The BIM considering the direct path and the multipath from the k-th wall is then given by,

$$\mathbf{B}_k = \iint_{x_t=x_{min}, y_t=y_{min}}^{x_{max}, y_{max}} \mathbf{F}_k(x_t, y_t)\, \mathrm{d}x_t\, \mathrm{d}y_t, \quad k = 1, 2, 3. \quad (11)$$

Like the classical CRBs, the BCRBs are present on the diagonals of the inverted BIMs. Unlike the FIMs, the BIMs are not a function of the target position vector, $\mathbf{x_t}$; tbut rather of the radar location $\mathbf{x_r}$.

Some of the double integrals for computing the BIMs are intractable and expressed as integrals of elliptic integrals [19]. For example, consider the element in the first row, first column of matrix $\mathbf{B}_k, k = 1, 2, 3$. It is readily shown that the following term is required to obtain the BIMs: $I_a = \iint_{x_t=x_{min}, y_t=y_{min}}^{x_{max}, y_{max}} \frac{x_r^2 - x_t^2 \quad \mathrm{d}x_t\, \mathrm{d}y_t}{||\mathbf{x_t}-\mathbf{x_r}||\, ||\mathbf{x_r^1}-\mathbf{x_t}||}$ The inner integral w.r.t x_t above can be evaluated using the incomplete elliptic integral of the first and the second kind [19], $F(\cdot, \cdot)$ and $E(\cdot, \cdot)$ respetively, and is not shown here due to space constraints.

There exist many such terms which are evaluated as integrals of $F(\cdot, \cdot)$ and $E(\cdot, \cdot)$. Numerical integration is employed in evaluating the BIMs since the incomplete elliptic integrals are themselves evaluated numerically, see [19] and references therein.

4. TARGET OR SENSOR POSITIONING USING STATISTICAL EXPERIMENTAL DESIGN

The FIMs and BIMs not only provide us with theoretical bounds on localization error variance, but they may also be of use in designing radar experiments which seek to maximize the ability to exploit multipath. That is, radar operators may wish to either determine where targets are best localized, or where sensors must be placed in order to best localize. These optimizations may be posed in terms of statistical experimental design theory [11].

Optimal positions for target localization given fixed radar position. Consider only a single wall, as in Fig. 1(a), with corresponding FIM $\mathbf{F}_1(\mathbf{x_t})$. The radar operator wants to know *a priori* where the target is best localized via multipath exploitation. Although in practice this is of course not in our control, but rather useful to know since estimated locations in the vicinity or at the optimal positions could be assigned as high confidence targets. Let us consider the *D*-optimal design [11], expressed as

$$\max_{\mathbf{x_t}} \det \mathbf{F}_1(\mathbf{x_t}), \quad (12)$$
$$\text{s.t} \quad y_A(\mathbf{x_r}, \mathbf{x_t}) \leq D_2 + D_y + y_r,\ -y_A(\mathbf{x_r}, \mathbf{x_t}) \leq -(D_y + y_r)$$

Solving (12) via the Karush-Kuhn-Tucker (KKT) conditions, there exist multiple optimal solutions for $\mathbf{x_t}$ which must satisfy

$$x_t^2 + (y_t - y_r)^2 - x_r^2 = 0, \quad \mathbf{A}_1\mathbf{x_t} + \mathbf{b}_1 \leq \mathbf{0} \quad (13)$$

where $\mathbf{A}_1 := \begin{bmatrix} -(D_2 + D_y) & x_r \\ D_y & -x_r \end{bmatrix}, \mathbf{b}_1 := [-x_r(D_2 + D_y + y_r), x_r(D_y + y_r)]^T$. In (13) the first condition is an equation of a circle, whereas the second is the affine inequality constraint which is identical to the multipath preserver in (5) but in matrix form. Using the same approach, i.e. when we optimize $\mathbf{F}_k(\mathbf{x_t}), k = 2, 3$ instead, the corresponding circles are given by

$$\text{For } \mathbf{F}_2 : (x_t + x_r)^2 + (y_t - D_2 - D_y - y_r)^2 - (D_2 + D_y)^2 = 0$$
$$\text{For } \mathbf{F}_3 : (x_t + D_1)^2 + (y_t - y_r)^2 - (D_1 - x_r)^2 = 0. \quad (14)$$

The optimal target locations w.r.t. these walls must satisfy their corresponding circles in (14) and multipath preservers in (6), respectively. These optimal circles comprising the optimal target locations follow a simple pattern: *from the radar at $\mathbf{x_r}$ draw three lines, one to each wall, or its imaginary extension, which intersects it at a 90 degree angle. Then, the points of intersections with the walls or their extensions are the respective centers of the circles, and the distance of the centers from the radar location are the respective radii.* It is further stressed that these optimal circles in (13) and (14) are not to be confused with the iso-range contours or (constant range) loci traced by the target, as in (2).

The optimal target location w.r.t the full FIM (i.e. all walls together), is expressed as:

$$\max_{\mathbf{x_t}} \det \mathbf{F}(\mathbf{x_t}), \quad (15)$$
$$\begin{aligned}\text{s.t} \quad & y_A(\mathbf{x_r}, \mathbf{x_t}) \leq D_2 + D_y + y_r,\ -y_A(\mathbf{x_r}, \mathbf{x_t}) \leq -(D_y + y_r)\\ & x_B(\mathbf{x_r}, \mathbf{x_t}) \leq D_1,\ -x_B(\mathbf{x_r}, \mathbf{x_t}) \leq 0\\ & y_C(\mathbf{x_r}, \mathbf{x_t}) \leq D_2 + D_y + y_r,\ -y_C(\mathbf{x_r}, \mathbf{x_t}) \leq -(D_y + y_r).\end{aligned}$$

A closed form solution as in (13),(14) is intractable for (15) and is shown numerically in the simulations.

Optimal radar position for Bayesian target localization. Now consider positioning the sensor, when one has some form of *a priori*

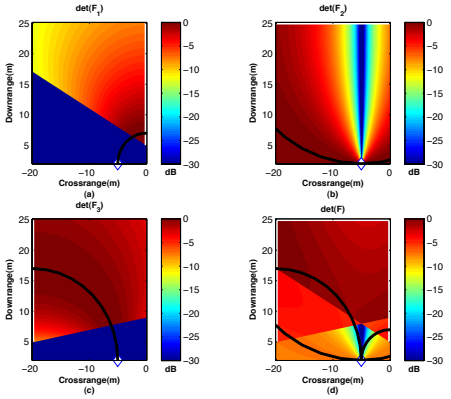

Fig. 2: Target Positioning:-walls (in white), For: (a) w1, (b) w2, (c) w3, (d) all, Radar ($\Diamond$). Deep nulls in (a,c) result because the corresponding multipath preservers are 0. Part of the optimal circles (solid black) as in (13),(14) are also shown.

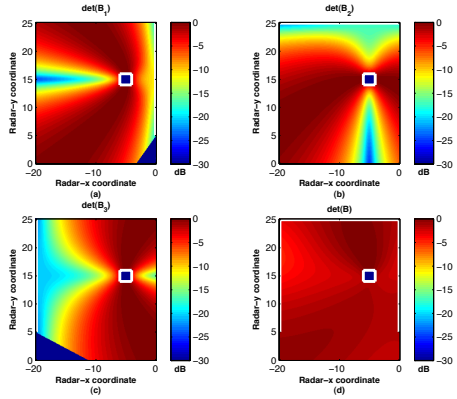

Fig. 3: Sensor Positioning (BIM):-walls (in white), For: (a) w1, (b) w2, (c) w3, (d) all, Target prior ($\square$). Deep nulls in (a,c) result because the corresponding multipath preservers are 0.

knowledge of the target location. We start again by designing the best sensor position in the presence of one of the three walls at a time, i.e. we express this as three separate optimization problems:

$$\begin{aligned} &\max_{\mathbf{x_r}} \det \mathbf{B}_k(\mathbf{x_r}), k = 1, 2, 3 \\ \text{s.t} \quad &\mathbf{x_r} \notin \aleph_p, \text{and } \mathbf{x_r} \in \Phi_k(\mathbf{x_t}) \end{aligned} \tag{16}$$

where, $\aleph_p := \text{supp}\, p(x_t, y_t)$ and

$$\begin{aligned} \Phi_1(\mathbf{x_t}) &:= \{\mathbf{x} | D_y + y_r \leq y_A(\mathbf{x}, \mathbf{x_t}) \leq D_2 + D_y + y_r,\ \mathbf{x_t} \in \aleph_p\} \\ \Phi_2(\mathbf{x_t}) &:= \{\mathbf{x} | 0 \leq x_B(\mathbf{x}, \mathbf{x_t}) \leq D_1,\ \mathbf{x_t} \in \aleph_p\} \\ \Phi_3(\mathbf{x_t}) &:= \{\mathbf{x} | D_y + y_r \leq y_C(\mathbf{x}, \mathbf{x_t}) \leq D_2 + D_y + y_r,\ \mathbf{x_t} \in \aleph_p\}. \end{aligned}$$

The first constraint in (16) states that the radar position cannot be in the target prior pdf support. The second constraint states that a radar position is considered feasible if *all* target positions within the prior pdf's support satisfy their respective multipath preservers.

The sensor positioning optimization for the general BIM (all walls together) is

$$\begin{aligned} &\max_{\mathbf{x_r}} \quad \det \mathbf{B}(\mathbf{x_r}) \\ \text{s.t} \quad &\mathbf{x_r} \notin \aleph_p, \text{ and } \mathbf{x_r} \in \bigcup_{k=1}^{3} \Phi_k(\mathbf{x_t}). \end{aligned} \tag{17}$$

The first constraint in (17) is identical to that in (16). The second constraint states that a radar position is considered feasible if it belongs to least one of the $\Phi_k, k = 1, 2, 3$, as defined in (16). A closed form solution to both (16) and (17) is not possible, and the optimization will be performed numerically in the simulations section. It is noted that (12),(15)-(17) may be performed performed offline, i.e. during the sensor deployment phase.

5. SIMULATIONS

The standoff distance, $D_y = 3$m is and noise variance $\sigma_p^2 = \sigma^2, p = 1, \ldots, 7$. Consider Fig. 2, which shows the determinant of the FIMs when the radar is assumed to be at position $\mathbf{x_r} = [-5, 2]^T$. The target position is varied in downrange and crossrange inside the urban canyon whose dimensions are $D_1 = D_2 = 20$m. In these figures the determinant of the FIMs are first normalized by their maximum value and depicted in the dB scale. In Fig. 2(a) we consider the direct path and the multipath from the the first wall (w1) only, and $\det(\mathbf{F}_1)$ is shown for varying target positions. The determinants of the FIMs w.r.t to the wall 2,3 are shown in Fig. 2(b-c). The determinant of the FIM when all the walls are considered is shown in Fig. 2(d). When considering walls 1, 2, or 3 individually, there exist several optimal target locations which maximize the determinant of their corresponding FIMs. As derived in (13) and (14), the optimal locations lie on circles which are also shown in Fig. 2(a-c). The corresponding circles are also shown in Fig. 2(d). Interestingly, it is seen that the optimal locations lie above the intersection of these circles, and are closer to wall-3 and wall-1. A final important phenomenon is seen from Fig. 2(b): a deep notch all along the radar's crossrange position is observed. This is the shadow region, i.e. a region where, if a target was present, nothing behind it would be seen by the radar. Interestingly, the design criteria chooses this as a multipath blind zone even though the multipath preserver formulation for the back wall does not take into account whether the point of reflection is in the shadow region; the experimental design does.

The application of sensor positioning via experimental design is demonstrated next. In Fig. 3(a-c), the determinant of the BIMs are shown when walls 1, 2, and 3 are considered independently, and in Fig. 3(d) when they are considered together. In these figures, the target prior pdf is uniformly distributed over the square with $(x_{max}, x_{min}) = (6, 4)$ and $(y_{max}, y_{min}) = (16, 14)$, as shown by $\square$. The shadow region notches are now clearly seen in Fig. 3(a-c). If the sensor is placed at these notches, then those corresponding multipath delays will not exist and cannot be used for subsequent exploitation. As noted from the prior simulation, these shadow region notches are placed automatically by the experimental design criteria and not by the multipath preservers. We see from Fig. 3(d), that some of the optimal sensor positions are inside the canyon, and close to the target prior region. It is noteworthy that these optimal sensor positions are not on the boresight(s) of the target prior region. For covertness, it is clear from Fig. 3(d) that the optimal sensor positions outside the canyon, and away from the target prior will be preferred.

6. SUMMARY

Bayesian as well as the classical Cramér-Rao lower bounds for the single sensor localization employing multipath exploitation were derived. A single target in a rectangular urban canyon and comprised of three walls was assumed. It was shown that each contributing multipath source, namely the walls, increases the Fisher information therefore improving the CRBs and BCRBs.

7. REFERENCES

[1] P. Setlur, G. E. Smith, F. Ahmad, and M. Amin, "Target localization with a single sensor via multipath exploitation," *IEEE Trans. Aerospace and Electron. Syst.*, vol. 43, no. 3, pp. 1996-2014, Jul. 2012.

[2] T. G. Farr, "Radar interactions with geologic surfaces," in *Guide to Magellan Image Interpretation*, NASA/JPL, 1993.

[3] E. I. Thorsos, "The validity of the Kirchhoff approximation for rough surface scattering using a Gaussian roughness spectrum," *Journ. Acoust. Soc. of Amer.*, vol. 83, no. 1, pp. 78-92, Jan. 1988.

[4] A. Tabatabaeenejad and M. Moghaddam,"Bistatic scattering from three-dimensional layered rough surfaces," *IEEE Trans. GeoSci. Rem. Sen.*, vol. 44, no. 8, pp. 2102-2114, Aug. 2006.

[5] S. O. Rice, "Reflection of Electromagnetic waves from slightly rough surfaces," *Comm. Pure Appl. Math*, vol. 4, no. 2/3, pp. 351-378, 1951.

[6] R. Linnehan, and J. Schindler, "Multistatic scattering from moving targets in multipath environments," *In Proc. IEEE Inter. Radar Conf.*, Pasadena, CA, 4-8 May 2009.

[7] S. Sen, M. Hurtado, A. Nehorai, "Adaptive OFDM radar for detecting a moving target in urban scenarios," *In Proc. Inter. Waveform Diversity and Design Conf.*, Orlando, FL, 8-13 Feb. 2009.

[8] B. Chakraborty, Y. Li, J. J. Zhang, T. Trueblood, A. Papandrous-Suppappola, and D. Morell, "Multipath exploitation with adaptive waveform design for tracking in urban terrain," *In Proc. IEEE Inter. Conf. Acost., Speech, and Signal process.*, Dallas, TX, 14-19 March 2010.

[9] J. L. Krolik, J. Farell, and A. Steinhardt, "Exploiting multipath propagation for GMTI in urban environments," *In Proc. IEEE Radar Conf.*, Verona, NY, 24-27 Apr. 2006

[10] D. Deiana, A. S. Kossen, and W. L. van Rossum, "Multipath exploitation in an urban environment using a MIMO survelillance radar," *In Proc. International Radar Conf.*, Vilnius, Lithuania, 16-18 June 2010.

[11] A. Atkinson, A. Donev, and R. Tobias, *Optimum experimental Design, with SAS*, Oxford University Press, Oxford, England, July 2007.

[12] A. I. Khuri, "A Note on D-Optimal Designs for Partially Nonlinear Regression Models," *Technometrics*, vol. 26, no. 1, pp. 59-61, Feb. 1984.

[13] B. M. Sadler and R. J. Kozick, "A survey of time delay estimation performance bounds," *In Proc. IEEE Workshop Sensor Array Multi- channel Signal Processing*, pp. 282288, Waltham, MA, Jul. 2006.

[14] K. W. K. Liu, and H. C. So, "Range-based source localisation with pure reflector in presence of multipath propagation," *Electron. Lett.*, vol. 46, no. 13, pp. 957-958, Jun. 2010.

[15] T. Dogaru, and C. Le, "SAR images of rooms and buildings based on FDTD computer models," *IEEE Trans. GeoSci. and Rem. Sen.*, vol. 47, no. 5, pp. 1388-1401, May 2009.

[16] P. Setlur, M. Amin and F. Ahmad, " Multipath Model and Exploitation in Through-the-Wall and Urban Radar Sensing," *IEEE Trans. GeoSci. and rem. Sensing*, vol. 49, no. 10, pp. 4021-4034, Oct. 2011.

[17] G. E. Smith and B. G. Mobasseri, "Multipath exploitation for radar target classification," *In Proc. IEEE Inter. Radar Conf.*, Atlanta GA, 7-11 May 2012.

[18] H. L. Van Trees, *Detection Estimation and Modulation Theory, Part I*, Wiley-Interscience, Sep. 2001.

[19] *Digital Library of Mathematical Functions*, National Inst. of Standards and Tech., 2011, available at `http://dlmf.nist.gov/`.